aerospace

MDPI

Article

Field-to-View Constrained Integrated Guidance and Control for Hypersonic Homing Missiles Intercepting Supersonic Maneuvering Targets

Zhibing Li [1], Quanlin Dong [1], Xiaoyue Zhang [1,*], Huanrui Zhang [1] and Feng Zhang [2]

[1] School of Instrumentation and Optoelectronic Engineering, Beihang University, Beijing 100191, China
[2] China North Industries Corp., Beijing 100029, China
* Correspondence: zhangxiaoyue@buaa.edu.cn; Tel.: +86-010-8231-6547

Abstract: An integrated guidance and control (IGC) scheme considering the field-of-view (FOV) constraint is proposed in this paper for hypersonic skid-to-turn (STT) missiles with a strapdown seeker intercepting a high-speed maneuvering target, which is based on the backstepping control (BC), barrier Lyapunov function (BLF), sliding mode control (SMC), dynamic surface control (DSC), and reduced-order extended state observer (ESO). First, a fifth-order strict feedback IGC model considering the rudder delay dynamics is derived, which also considers the drag effect on the axial velocity. Second, the missile guidance control system based on the BC consists of seeker, guidance, angle-of-attack, attitude, and rudder subsystems. The seeker subsystem was designed based on the BLF, and the other four subsystems were designed based on the SMC. The system-lumped disturbances, including unknown target maneuvers, unmodeled parts, perturbations caused by aerodynamic parameter variations, and external disturbances, were estimated and compensated for using the reduced-order ESO. The DSC prevented the "differential explosion" caused by virtual control commands introduced by the BC. Subsequently, the stability of the closed-loop system was strictly proven using the Lyapunov theory, and the boundedness of the FOV angle was strictly derived. Finally, the simulation results demonstrated the effectiveness and robustness of the proposed IGC scheme.

Keywords: integrated guidance and control; hypersonic homing missiles; barrier Lyapunov function; backstepping control; reduced-order ESO

check for updates

Citation: Li, Z.; Dong, Q.; Zhang, X.; Zhang, H.; Zhang, F. Field-to-View Constrained Integrated Guidance and Control for Hypersonic Homing Missiles Intercepting Supersonic Maneuvering Targets. *Aerospace* **2022**, *9*, 640. https://doi.org/10.3390/aerospace9110640

Academic Editor: Piotr Lichota

Received: 21 September 2022
Accepted: 21 October 2022
Published: 24 October 2022

Publisher's Note: MDPI stays neutral with regard to jurisdictional claims in published maps and institutional affiliations.

Copyright: © 2022 by the authors. Licensee MDPI, Basel, Switzerland. This article is an open access article distributed under the terms and conditions of the Creative Commons Attribution (CC BY) license (https://creativecommons.org/licenses/by/4.0/).

1. Introduction

Emergency maneuver avoidance is common for general maneuvering targets when missile interception is encountered. There are new requirements for missile speed and maneuverability, as the target has increased speed and maneuverability. It is challenging to design a missile guidance control system (GCS) for hypersonic missiles that can precisely intercept high-speed and highly maneuvering targets [1]. In particular, it is highly likely to result in a large field-of-view (FOV) angle owing to the target maneuvering during pursuit. Both gimbaled and strapdown seekers have a limited FOV range [2]. The gimbaled seeker is fixed to an inertial pedestal with a stabilization loop to isolate body movements and a tracking loop to maintain the seeker axis along the missile–target line [3]. It has a wide FOV range, and can directly measure the line-of-sight (LOS) angular rate required by the guidance law. The disadvantages are its complex structure and high cost. In contrast, the strapdown seeker is fixed directly to the missile body and has attracted considerable attention over the years because of its compact structure, high reliability, low cost, and unlimited tracking rate [4]. Unlike the gimbaled seeker, the strapdown seeker is coupled with attitude data of the body, so only the body LOS (BLOS) is measurable, and it often needs to be decoupled when designing the GCS [5]. However, the FOV range of strapdown seekers is smaller. During the pursuit of a maneuvering target, the missile must constantly

adjust its body attitude to generate a large overload and achieve precision strikes. This can easily cause an extreme FOV angle during the homing phase and thus a loss of the target, resulting in mission failure.

The design of a GCS that considers the FOV constraint has received considerable attention, and most of the research focuses on the design of guidance laws. In [6], a guidance law that considers FOV constraints was proposed for maneuvering targets. The FOV angle is equivalent to the missile look angle (the angle between the missile velocity and the missile–target LOS), based on the assumption that the angle of attack is sufficiently small. This guidance law ensures that the missile look angle is within a certain range by constructing a sliding mode surface and introducing a sigmoid function. Kim and Lee [7] proposed a guidance law based on optimal control to achieve the narrow FOV constraint for homing missiles. In [8], the FOV constraint is equivalently transformed into a time-varying asymmetric constraint on the missile–target relative velocity perpendicular to the LOS, and the guidance law was designed based on the dynamic surface control (DSC) and time-varying asymmetric barrier Lyapunov function (BLF), which achieves not only the FOV constraint but also the impact angle constraint. In [9], a double-constrained guidance law with seeker FOV and impact angle constraints was proposed. This law is realized by introducing a hyperbolic tangent function to design the virtual guidance law and one-to-one nonlinear mapping. Zhou and Hu [10] used a quadratic Lyapunov function and an integral Lyapunov function to implement the guidance law with dual constraints of the seeker FOV angle and impact angle constraint for variable speed conditions. In [11], the guidance law with FOV and impact time constraints was implemented by defining two time-varying sliding mode surfaces. Han and Hu [12] achieved the seeker FOV angle constraint together with the impact time and angle constraints. In [13], a cooperative guidance law was proposed to ensure the attack of multiple missiles on a stationary target with a guaranteed FOV constraint. In [14], an optimal guidance law based on optimal control theory was proposed for the homing phase. It comprises an acceleration command to guarantee the maximum look angle in the initial phase, an acceleration command to guarantee the look angle constraint in the homing phase, and an acceleration command to achieve the impact angle constraint.

In summary, the above guidance laws considering the FOV constraint assume that the angle of attack is sufficiently small, in which case the look angle of missiles can be equivalent to the BLOS, and the FOV constraint and precise interception can be achieved by constraining the look angle of missiles. However, this assumption is tantamount to ignoring the attitude dynamics of the missiles. In the actual interception, to achieve precise interception it is necessary to adjust the speed direction constantly, and the missile speed variation is a result of the combined effect of the missile lift and gravity, whereas the missile lift is mainly dependent on the angle of attack. When a missile has to perform large angle-of-attack maneuvers in an intercept scenario, the assumption does not hold. The FOV constraint is likely to be violated in an interception, or it will fail to intercept. Therefore, such an assumption is too ideal to be realized in the flight control of missiles.

Another disadvantage of the aforementioned guidance laws, which are designed for the missile guidance loop, is that the dynamic characteristics of the autopilot are ignored. The guidance loop and control loop are designed separately (SGC) in a traditional manner for the GCS of missiles and then matched together. This method is based on the assumption of spectral separation, and its main drawback is that it ignores the coupling effect between the two subsystems [15]. The SGC method is effective for low-velocity missiles. However, for the terminal guidance phase of a hypersonic missile to intercept a high-speed maneuvering target, the design of the GCS is challenging because of its fast time-varying and strongly nonlinear system states [16]. In this case, the assumption of spectrum separation was no longer valid. If the SGC method is used to design the GCS, the interception performance may degrade, and the GCS may be unstable when intercepting a high-speed maneuvering target. In contrast, the integrated guidance and control (IGC) method can directly generate control commands based on missile system states and missile–

target relative motion states. This method fully considers the coupling effects of guidance and control subsystems. This is a very effective way to solve the problem of the degraded GCS performance generated by the SGC method [17]. In addition, the IGC method can shorten the development cycle, improve the economy and reliability, and improve the stability of the GCS [18].

Because the IGC method treats the guidance and control loops as a whole, the GCS itself is a high-order nonlinear system. There are also mismatched uncertainties caused by target maneuvers, time-varying parameter perturbations, and external disturbances, which will create many difficulties for the controller design when considering design constraints, such as the impact angle constraint or FOV constraint [19]. In recent years, many studies have explored the IGC method considering the FOV constraint and have achieved some results. In [20], an IGC method considering the FOV constraint was proposed for missiles with a strapdown seeker, using the BLOS angle as a system state and establishing a functional relationship with the LOS angle. The integral BLF was used to ensure that the BLOS angle was within the given constraint range. In [21], an IGC model was simplified by introducing an axial overload, and an IGC method considering the FOV constraint was proposed based on the DSC and integral BLF. Based on this, a new IGC scheme considering the FOV constraint was proposed in the literature [22] for striking a stationary or moving target based on the output-to-input saturation transformation (OIST) technique, which can be applied to the entire homing phase without the assumption of a small angle of attack. In [23], a three-dimensional low-order IGC model considering the FOV constraint was established, and a three-dimensional IGC scheme based on an integral BLF was proposed.

In summary, the subjects of the mentioned IGC schemes considering the FOV constraint are all subsonic or supersonic missiles with a strapdown seeker, which mainly uses the BLF to ensure that the BLOS angle does not exceed its maximum FOV angle. They are all based on the assumption that the control command is the rudder angle; that is, the delayed dynamic characteristics of the rudder are ignored. However, the flight speed of hypersonic interceptor missiles exceeds Mach 5. The system states are rapidly time-varying in the terminal phase. In particular, as it is the only actuator of the missile in the terminal guidance phase, the delayed dynamic characteristics of the rudder will seriously affect the missile body's response speed. Therefore, thought should be given to increasing the designed controller's performance. In this paper, a new IGC scheme considering the FOV constraint is proposed based on backstepping control (BC), DSC, and BLF for intercepting a high-speed maneuvering target using a hypersonic skid-to-turn (STT) missile with a strapdown seeker. Unlike the guiding law design, the assumption of a small angle of attack was avoided. In contrast to other works [20–23], the striking of a hypersonic missile intercepting a high-speed maneuvering target was studied, and the important part was to simplify the rudder as a first-order delay model. The rudder angle was then taken as the system state of the IGC model. Inspired by the literature [20], we solved the strapdown seeker FOV constraint using the BLF. Furthermore, the lumped system disturbances, including aerodynamic parameter perturbations, unmodeled parts of the system, external disturbances, and target maneuverability, were accurately estimated using the reduced-order extended state observer (ESO). The main contributions of this study that distinguish it from previous works are as follows:

1. In contrast to the literature [17,24], based on the BLOS, LOS angular rate, angle of attack, pitch angle rate, and rudder angle, a strict-feedback nonlinear IGC pursuit model under the variable-speed condition is established, which considers the aerodynamic drag and omits the assumption of a small angle of attack.
2. Based on the BC, BLF, and DSC, a new IGC controller is proposed to achieve precise hitting of a supersonic maneuvering target by a hypersonic missile, where the BLF is introduced to ensure that the FOV constraint is realized. The lumped disturbances in each loop of the system model were estimated using the reduced-order ESO and compensated in the controller to enhance robustness.

3. The stability of the closed-loop system was strictly proven using the Lyapunov theory, and the boundedness of the FOV angle was theoretically proven. The simulation results further verified the effectiveness and robustness of the proposed IGC scheme.

The remainder of this paper is organized as follows. The derivation of the IGC model is presented in Section 2. Section 3 introduces the proposed IGC scheme for strapdown missiles. A closed-loop system stability analysis is presented in Section 4. The simulation results and analysis are presented in Section 5. Finally, Section 6 summarizes the conclusions of this study.

2. Problem Formulation

In this section, the missile dynamics and geometric equations, first-order dynamics model of the rudder, and missile–target engagement kinematics are first elaborated, and the missile IGC model is subsequently derived.

2.1. IGC Model Derivation

The missile–target engagement geometry for the strapdown missile in the pitch plane is shown as Figure 1, where M and T represent the missile and target, respectively. R is the relative distance along the LOS. V_M and V_T denote the velocities of the missile and target, respectively, and their flight path angles are θ_M and θ_T. (x_M, y_M) and (x_T, y_T) denote the positions of the missile and target in the inertial coordinate system, respectively. The missile axial acceleration and normal acceleration are represented as a_M^X and a_M^Y, respectively. Similarly, the target axial acceleration and normal acceleration are denoted as a_T^X and a_T^Y, respectively. x_B represents the missile body axis, q_B the BLOS angle, q_L the LOS angle, ϑ the missile pitch angle, and α the angle of attack.

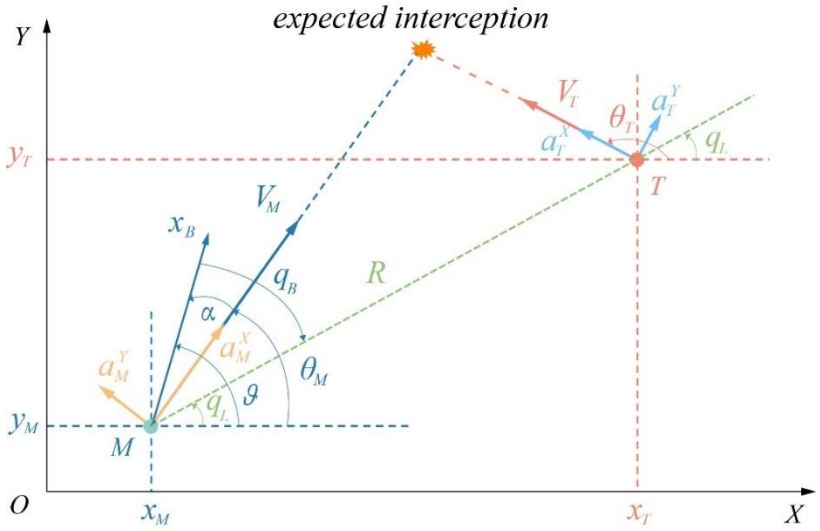

Figure 1. Two-dimensional missile–target engagement geometry for the strapdown missile.

The missile–target engagement dynamics are formulated as follows:

$$\dot{R} = V_T \cos(\theta_T - q_L) - V_M \cos(\theta_M - q_L) \tag{1}$$

$$R\dot{q}_L = V_T \sin(\theta_T - q_L) - V_M \sin(\theta_M - q_L) \tag{2}$$

Differentiating Equation (2) combining with Equation (1) yields

$$R\ddot{q}_L + \dot{R}\dot{q}_L = -\dot{R}\dot{q}_L - a_M^Y \cos(\theta_M - q_L) - a_M^X \sin(\theta_M - q_L) + d_T \tag{3}$$

where $a_M^Y = V_M\dot{\theta}_M$, $a_M^X = \dot{V}_M$, $d_T = a_T^Y \cos(\theta_T - q_L) + a_T^X \sin(\theta_M - q_L)$ is the uncertain term caused by the unknown target acceleration, $a_T^Y = V_T\dot{\theta}_T$, and $a_T^X = \dot{V}_T$.

The planar nonlinear missile dynamics and geometric equation are as follows:

$$\alpha = \vartheta - \theta_M \tag{4}$$

$$\dot{\vartheta} = \omega_z \tag{5}$$

$$a_M^Y = V_M \dot{\theta}_M = \frac{T \sin\alpha + Y}{m} - g\cos\theta_M \tag{6}$$

$$a_M^X = \dot{V}_M = \frac{T\cos\alpha - D}{m} - g\sin\theta_M \tag{7}$$

$$J_z \dot{\omega}_z = M_0(\alpha, \omega_z, \delta_z) \tag{8}$$

The lift force and pitch moment are described as

$$\begin{cases} Y = QS(c_y^\alpha \alpha + c_y^{\delta_z}\delta_z) \\ D = c_{x0}QS + c_x^{\alpha^2} QS\alpha^2 \end{cases} \tag{9}$$

$$\begin{cases} M_0 = M_\alpha \alpha + M_{\omega_z}\omega_z + M_{\delta_z}\delta_z \\ M_\alpha = QSlm_z^\alpha \\ M_{\omega_z} = \frac{QSl^2 m_z^{\omega_z}}{V_M} \\ M_{\delta_z} = QSlm_z^{\delta_z} \end{cases} \tag{10}$$

From the geometry in Figure 1, it can be deduced that

$$q_B = q_L - \vartheta \tag{11}$$

Defining $d_1 = -\omega_z$, differentiating Equation (11), and combining with Equation (5) yields

$$\dot{q}_B = \dot{q}_L + d_1 \tag{12}$$

According to Equations (6), (7) and (9), and neglecting the small terms, the missile axial and normal accelerations can be approximated as

$$\begin{cases} a_M^X = \dot{V}_M = \frac{T\cos\alpha}{m} - \frac{c_{x0}QS + c_x^{\alpha^2}QS\alpha}{m} - g\sin\theta_M + d_{a_M^X} \\ a_M^Y = V_M\dot{\theta}_M = \frac{T\sin\alpha}{m} + \frac{QSc_y^\alpha}{m}\alpha - g\cos\theta_M + d_{a_M^Y} \end{cases} \tag{13}$$

where $d_{a_M^X}$ and $d_{a_M^Y}$ denote approximation errors.

Assumption 1. *The engine thrust is 0 in the terminal guidance phase, i.e.,* $T = 0$.

Substituting Equation (13) into Equation (3) yields

$$\begin{aligned} R\ddot{q}_L + \dot{R}\dot{q}_L &= -\dot{R}\dot{q}_L - \cos(\theta_M - q_L)[\tfrac{QSc_y^\alpha}{m}\alpha - g\cos\theta_M + d_{a_M^Y}] \\ &\quad + \sin(\theta_M - q_L)[\tfrac{c_{x0}QS}{m} + \tfrac{c_x^{\alpha^2}QS}{m}\alpha + g\sin\theta_M - d_{a_M^X}] + d_T \\ &= -\dot{R}\dot{q}_L + g\cos\theta_M\cos(\theta_M - q_L) + (\tfrac{c_{x0}QS}{m} + g\sin\theta_M)\sin(\theta_M - q_L) \\ &\quad + [\tfrac{c_x^{\alpha^2}QS}{m}\sin(\theta_M - q_L) - \tfrac{QSc_y^\alpha}{m}\cos(\theta_M - q_L)]\alpha + d_2(d_{a_M^Y}, d_{a_M^X}, d_T) \end{aligned} \tag{14}$$

where $d_2(d_{a_M^Y}, d_{a_M^X}, d_T)$ is the lumped disturbance, which contains unmodeled parts of the system, perturbations caused by time-varying aerodynamic parameters, and uncertain terms caused by the target maneuvers.

Remark 1. *Owing to the rudder mechanical structure, in addition to the limitation of the maximum rudder angle, the dynamic delay between the actual rudder command and the rudder angle must be considered owing to the fast time-varying characteristics in the terminal guidance phase, which are ignored in most of the literature.*

The rudder system model can be approximated as

$$\delta_{zc} = \tau_z \dot{\delta}_z + \delta_z \tag{15}$$

Owing to the physical limitations of the actuator, the saturation constraint of the rudder deflection angle can be expressed as

$$sat(\delta_{zc}) = \begin{cases} \delta_{zc}^{\max} sign(\delta_z), \text{ if } |\delta_{zc}| > \delta_{zc}^{\max} \\ \delta_{zc}, \text{if } |\delta_{zc}| \leq \delta_{zc}^{\max} \end{cases} \tag{16}$$

To simplify the equations, the system parameters are redefined as follows:

$$a_1 = \frac{QSc_{x0}}{m}, a_2 = \frac{QSc_x^{\alpha^2}}{m}, a_3 = \frac{QSc_y^{\alpha}}{m}, a_4 = \frac{QSc_y^{\delta_z}}{m},$$
$$a_5 = \frac{QSlm_z^{\alpha}}{J_z}, a_6 = \frac{QSl^2 m_z^{\omega_z}}{J_z V_M}, a_7 = \frac{QSlm_z^{\delta_z}}{J_z}, a_8 = \frac{1}{\tau_z}$$

Defining the state vector $\mathbf{X} = [x_1, x_2, x_3, x_4, x_5] = [q_B, \dot{q}_L, \alpha, \omega_z, \delta_z]$ and the control input $u = \delta_{zc}$, the IGC model for the strapdown missile with strict-feedback state questions can be formulated as

$$\begin{cases} \dot{x}_1 = b_1 x_2 + d_1 \\ \dot{x}_2 = f_2(x_2) + b_2 x_3 + d_2 \\ \dot{x}_3 = f_3(x_3) + b_3 x_4 + d_3 \\ \dot{x}_4 = f_4(x_4) + b_4 x_5 + d_4 \\ \dot{x}_5 = f_5(x_5) + b_5 u \end{cases} \tag{17}$$

where

$$\left\{ \begin{array}{l} b_1 = 1, d_1 = -\omega_z \\ f_2(x_2) = -\frac{2\dot{R}\dot{q}_L}{R} + \frac{g\cos\theta_M \cos(\theta_M - q_L) + (a_1 + g\sin\theta_M)\sin(\theta_M - q_L)}{R} \\ b_2 = \frac{a_2 \sin(\theta_M - q_L) - a_3 \cos(\theta_M - q_L)}{R}, d_2 = d_2\left(d_{a_{MS}^Y}, d_{a_{MS}^X}, d_T\right) \\ f_3(x_3) = -\frac{a_3}{V_M}\alpha + \frac{g\cos\theta_M}{V_M}, b_3 = 1, d_3 = d_\alpha \\ f_4(x_4) = a_5\alpha + a_6\omega_z, b_4 = a_7, d_4 = d_{\omega_z} \\ f_5(x_5) = -a_8\delta_z, b_5 = a_8 \end{array} \right\}$$

Assumption 2. *The lumped disturbances $d_i, i = 1, 2, \cdots, 4$ in system (17) and their first-order derivatives are bounded; however, the upper bounds are unknown.*

Remark 2. *d_1 is determined by the pitch angular velocity of the missile, d_2 is mainly determined by the unknown target acceleration, and d_3 and d_4 are more influenced by the perturbations caused by variation in the aerodynamic parameters. As the variations in the target maneuver, aerodynamic parameters, and missile attitude are all bounded, Assumption 2 is reasonable.*

2.2. IGC Controller Design Objective

The objectives of this study were to design an IGC controller for the strict feedback IGC model in Equation (17), which can satisfy the following requirements:

- The FOV constraint is satisfied during the entire interception; that is, $|x_1| < q_B^{\max}$, where $q_B^{\max}$ is the maximum seeker FOV angle.
- The desired terminal FOV angle converges to 0, i.e., $q_B \to q_{Bd} = 0$.
- The actuator dynamic characteristics are considered, and a small miss distance is achieved.
- All signals of the closed-loop system are uniform ultimately bounded.
- There is strong robustness in the face of multiple uncertainties.

3. IGC Controller Design

The derivation of the novel IGC controller is detailed in this section for the IGC model in Equation (17) with strict-feedback states, where the lumped disturbances in the system model are estimated and compensated for using a reduced-order ESO to enhance the controller robustness.

The BLF function is an efficient way to address the state constraint problem [25]. Thus, this study uses the BLF to ensure that the seeker FOV does not exceed the maximum FOV angle. As shown in Equation (17), the fifth-order strict-feedback IGC model is a time-varying nonlinear system with mismatched uncertainties. The GCS consists of seeker, guidance, angle-of-attack, attitude, and rudder subsystems based on the BC. Consequently, the BLF is used to design the seeker subsystem, and the sliding mode control (SMC) algorithm is used to design the other four subsystems. First-order filters obtain the virtual control command derivatives to prevent "differential explosions" caused by the BC.

Step 1: The first equation in Equation (17) is the seeker subsystem that guarantees that the BLOS angle does not exceed the maximum FOV angle by the BLF, that is, $|x_1| < k_{c1}$. To ensure the precise interception of a maneuvering target, the desired FOV angle is $x_{1d} = 0$. The first sliding mode surface is defined as

$$s_1 = x_1 - x_{1d} \tag{18}$$

According to Equation (18), $|s_1| < k_{c1} - 0 = k_{b1}$.

The BLF is defined as

$$V_{BLF} = \frac{1}{2} a_0 In \frac{k_{b1}^2}{k_{b1}^2 - s_1^2} \tag{19}$$

where $a_0 > 0$.

Differentiating Equation (19) yields

$$\begin{aligned} V_{BLF} &= \tfrac{a_0 s_1 \dot{s}_1}{k_{b1}^2 - s_1^2} = \tfrac{a_0 s_1 \dot{x}_1}{k_{b1}^2 - s_1^2} \\ &= \tfrac{a_0 s_1 [b_1 x_2 + d_1]}{k_{b1}^2 - s_1^2} \end{aligned} \tag{20}$$

According to Equation (20), the virtual control command x_{2c} is designed as follows:

$$x_{2c} = \frac{1}{b_1}(-d_1 - k_1 s_1) \tag{21}$$

where $k_1 > 0$.

The reduced-order ESO used to estimate the system lumped disturbance d_1 [26] can be formulated as follows:

$$\begin{cases} \dot{p}_1 = -\beta_1 p_1 - \beta_1{}^2 x_1 - \beta_1 b_1 x_2 \\ \widehat{d}_1 = p_1 + \beta_1 x_1 \end{cases} \tag{22}$$

where p_1 is the auxiliary variable, $\widehat{d}_1$ is the estimation of the lumped disturbance d_1, and $\beta_1 > 0$ is the observer gain to be designed.

Therefore, the virtual control command in Equation (21) can be rewritten as

$$x_{2c} = \frac{1}{b_1}(-\widehat{d}_1 - k_1 s_1) \tag{23}$$

To avoid the "differential explosion" caused by the BC, the DSC is adopted to make x_{2c} pass through a first-order filter to obtain x_{2d} and $\dot{x}_{2d}$.

$$\begin{cases} \tau_2 \dot{x}_{2d} + x_{2d} = x_{2c}, \\ x_{2d}(0) = x_{2c}(0) \end{cases} \tag{24}$$

where $\tau_2 > 0$ is the time constant.

Step 2: For the guidance subsystem (the second equation in Equation (17)), to ensure the tracking of x_2 to the virtual command x_{2d}, the second sliding mode surface is defined as

$$s_2 = x_2 - x_{2d} \tag{25}$$

Differentiating Equation (25), and combining the second equation in Equation (17) yields

$$\dot{s}_2 = \dot{x}_2 - \dot{x}_{2d} = f_2(x_2) + b_2 x_3 + d_2 - \dot{x}_{2d} \tag{26}$$

Choosing x_3 as the virtual control input that can be designed as follows:

$$x_{3c} = \frac{1}{b_2}[-f_2(x_2) - d_2 + \dot{x}_{2d} - k_2 s_2 - \frac{s_1}{k_{b1}^2 - s_1^2}] \tag{27}$$

where $k_2 > 0$.

Similarly, the reduced-order ESO used to estimate the lumped disturbance d_2 can be formulated as

$$\begin{cases} \dot{p}_2 = -\beta_2 p_2 - {\beta_2}^2 x_2 - \beta_2[f_2(x_2) + b_2 x_3] \\ \widehat{d}_2 = p_2 + \beta_2 x_2 \end{cases} \tag{28}$$

where p_2 is the auxiliary variable, $\widehat{d}_2$ is the estimation of the lumped disturbance d_2, and $\beta_2 > 0$ is the observer gain to be designed.

Equation (27) can be rewritten as

$$x_{3c} = \frac{1}{b_2}[-f_2(x_2) - \widehat{d}_2 + \dot{x}_{2d} - k_2 s_2 - \frac{s_1}{k_{b1}^2 - s_1^2}] \tag{29}$$

Letting x_{3c} pass through the first-order filter with the time constant $\tau_3 > 0$ yields x_{3d} and $\dot{x}_{3d}$.

$$\begin{cases} \tau_3 \dot{x}_{3d} + x_{3d} = x_{3c}, \\ x_{3d}(0) = x_{3c}(0) \end{cases} \tag{30}$$

Step 3: For the angle-of-attack subsystem (the third equation in Equation (17)), to ensure the tracking of x_3 to the virtual command x_{3d}, the third sliding mode surface is defined as

$$s_3 = x_3 - x_{3d} \tag{31}$$

Differentiating Equation (31), and combining the third equation in Equation (17) yields

$$\dot{s}_3 = \dot{x}_3 - \dot{x}_{3d} = f_3(x_3) + b_3 x_4 + d_3 - \dot{x}_{3d} \tag{32}$$

x_4 is selected as the virtual control input that can be designed as follows:

$$x_{4c} = \frac{1}{b_3}[-f_3(x_3) - d_3 + \dot{x}_{3d} - k_3 s_3] \tag{33}$$

where $k_3 > 0$.

The reduced-order ESO used to estimate the lumped disturbance d_3 can be formulated as

$$\begin{cases} \dot{p}_3 = -\beta_3 p_3 - {\beta_3}^2 x_3 - \beta_3[f_3(x_3) + b_3 x_4] \\ \widehat{d}_3 = p_3 + \beta_3 x_3 \end{cases} \tag{34}$$

where p_3 is the auxiliary variable, $\widehat{d}_3$ is the estimation of the lumped disturbance d_3, and $\beta_3 > 0$ is the observer gain to be designed.

Equation (33) can be rewritten as

$$x_{4c} = \frac{1}{b_3}[-f_3(x_3) - \widehat{d}_3 + \dot{x}_{3d} - k_3 s_3] \tag{35}$$

Letting x_{4c} pass through the first-order filter with the time constant $\tau_4 > 0$ yields x_{4d} and $\dot{x}_{4d}$.

$$\begin{cases} \tau_4 \dot{x}_{4d} + x_{4d} = x_{4c}, \\ x_{4d}(0) = x_{4c}(0) \end{cases} \tag{36}$$

Step 4: For the attitude subsystem (the fourth equation in Equation (17)), to ensure the tracking of x_4 to the virtual command x_{4d}, the fourth sliding mode surface is defined as

$$s_4 = x_4 - x_{4d} \tag{37}$$

Differentiating Equation (37), and combining the fourth equation in Equation (17) yields

$$\dot{s}_4 = \dot{x}_4 - \dot{x}_{4d} = f_4(x_4) + b_4 x_5 + d_4 - \dot{x}_{4d} \tag{38}$$

x_5 is selected as the virtual control input that can be designed as follows:

$$x_{5c} = \frac{1}{b_4}[-f_4(x_4) - d_4 + \dot{x}_{4d} - k_4 s_4] \tag{39}$$

where $k_4 > 0$.

The reduced-order ESO used to estimate the lumped disturbance d_4 can be formulated as

$$\begin{cases} \dot{p}_4 = -\beta_4 p_4 - \beta_4{}^2 x_4 - \beta_4[f_4(x_4) + b_4 x_5] \\ \widehat{d}_4 = p_4 + \beta_4 x_4 \end{cases} \tag{40}$$

where p_4 is the auxiliary variable, p_4 is the estimation of the lumped disturbance d_4, and $\beta_4 > 0$ is the observer gain to be designed.

Equation (39) can be rewritten as

$$x_{5c} = \frac{1}{b_4}[-f_4(x_4) - \widehat{d}_4 + \dot{x}_{4d} - k_4 s_4] \tag{41}$$

Letting x_{5c} pass through the first-order filter with the time constant $\tau_5 > 0$ yields x_{5d} and $\dot{x}_{5d}$.

$$\begin{cases} \tau_5 \dot{x}_{5d} + x_{5d} = x_{5c}, \\ x_{5d}(0) = x_{5c}(0) \end{cases} \tag{42}$$

Step 5: For the rudder subsystem (the fifth equation in Equation (17)), to ensure the tracking of x_5 to the virtual command x_{5d}, the fifth sliding mode surface is defined as

$$s_5 = x_5 - x_{5d} \tag{43}$$

Differentiating Equation (43) and combining the fifth equation in Equation (17) yields

$$\dot{s}_5 = \dot{x}_5 - \dot{x}_{5d} = f_5(x_5) + b_5 u - \dot{x}_{5d} \tag{44}$$

The desired controller input is designed as

$$u = \delta_{zc} = \frac{1}{b_5}[-f_5(x_5) + \dot{x}_{5d} - k_5 s_5] \tag{45}$$

where $k_5 > 0$.

The results are shown in Figure 2. The proposed IGC controller includes virtual control commands, and the control input can be summarized as follows:

$$\begin{cases} x_{2c} = \frac{1}{b_1}(-\widehat{d}_1 - k_1 s_1) \\ x_{3c} = \frac{1}{b_2}[-f_2(x_2) - \widehat{d}_2 + \dot{x}_{2d} - k_2 s_2 - \frac{s_1}{k_{b1}^2 - s_1^2}] \\ x_{4c} = \frac{1}{b_3}[-f_3(x_3) - \widehat{d}_3 + \dot{x}_{3d} - k_3 s_3] \\ x_{5c} = \frac{1}{b_4}[-f_4(x_4) - \widehat{d}_4 + \dot{x}_{4d} - k_4 s_4] \\ \delta_{zc} = \frac{1}{b_5}[-f_5(x_5) + \dot{x}_{5d} - k_5 s_5] \end{cases} \tag{46}$$

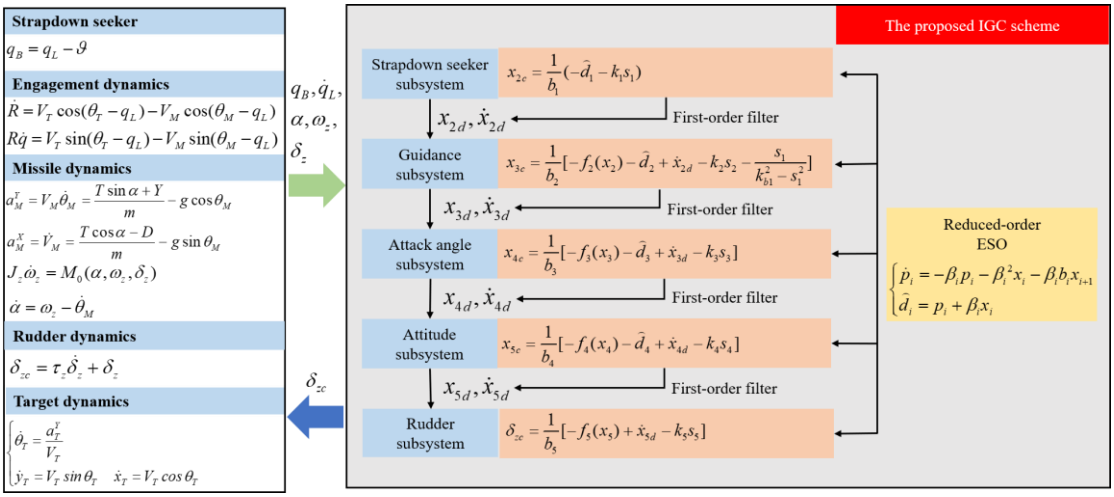

Figure 2. Configuration of the proposed IGC law based on BC with BLF and SMC.

4. Stability Analysis of the Closed-Loop System

In this section, the stability of the closed-loop system is proved using the Lyapunov theory. First, the following lemmas and assumptions are introduced to prove the system's stability.

Lemma 1. *For any $k_{bi} > 0$, satisfying $\forall|z_i| < k_{bi}$, $i = 1, 2, \cdots$, there is then*

$$\ln\left(\frac{k_{bi}^2}{k_{bi}^2 - z_i^2}\right) \leq \frac{z_i^2}{k_{bi}^2 - z_i^2}. \tag{47}$$

Lemma 2. *There exist observer gains $\beta_i, i = 1, 2, \cdots, 4$ for the reduced-order ESO in Equations (22), (28), (34) and (40) that make the observer estimations $\widehat{d}_i, i = 1, 2, \cdots, 4$ converge to the system-lumped disturbances $d_i, i = 1, 2, \cdots, 4$; that is, $\widehat{d}_1 \to d_1$, $\widehat{d}_2 \to d_2$, $\widehat{d}_3 \to d_3$, and $\widehat{d}_4 \to d_4$ [26].*

Lemma 3. *Under the conditions that the system states are continuous and bounded, there exists $\eta_i > 0, i = 2, 3, \cdots, 5$ such that $|\dot{x}_{ic}| \leq \eta_i$. Further, defining the filter errors as $e_{0i} = x_{id} - x_{ic}$, $i = 2, 3, \cdots, 5$, there are $e_{0i}\dot{e}_{0i} = -\frac{e_{0i}^2}{\tau_i} - e_{0i}\dot{x}_{ic}$, $i = 2, 3, \cdots, 5$ [27].*

Assumption 3. *At the initial time of the interception start, the target is captured by the missile seeker, and the FOV angle satisfies that $|q_B| \leq q_B^{\max}$.*

Assumption 4. *There exist the positive constants $R_{\min}$ and $R_{\max}$ in the terminal guidance phase, such that $0 < R_{\min} \leq R_{tf} \leq R_{\max}$ at the interception point and $\dot{R} < 0$ in the terminal guidance phase.*

Assumption 5. *When the missile–target distance is very close, the strapdown seeker is in the dead zone, and the BLOS angle is not available. Therefore, the designed controller only considers*

the situation when $R \geq R_{dz}$; $R_{dz} > 0$ is the minimum distance related to the dead zone of the strapdown seeker.

The Lyapunov function candidate is considered as

$$V_s = V_1 + V_2 + V_3 + V_4 + V_5 \tag{48}$$

where

$$V_1 = V_{BLF} + \frac{1}{2}e_{02}^2 + \frac{1}{2}\varepsilon_1^2 \tag{49}$$

$$V_2 = \frac{1}{2}s_2^2 + \frac{1}{2}e_{03}^2 + \frac{1}{2}\varepsilon_2^2 \tag{50}$$

$$V_3 = \frac{1}{2}s_3^2 + \frac{1}{2}e_{04}^2 + \frac{1}{2}\varepsilon_3^2 \tag{51}$$

$$V_4 = \frac{1}{2}s_4^2 + \frac{1}{2}e_{05}^2 + \frac{1}{2}\varepsilon_4^2 \tag{52}$$

$$V_5 = \frac{1}{2}s_5^2 \tag{53}$$

where $\varepsilon_i = d_i - \widehat{d}_i, i = 1, 2, \cdots, 4$ are the disturbance estimation errors.

According to [26], there is

$$\varepsilon_i\dot{\varepsilon}_i = \varepsilon_i(-\beta_i\varepsilon_i + \dot{d}_i), i = 1, 2, \cdots, 4 \tag{54}$$

According to Assumption 2, the lumped disturbances $\dot{d}_i, i = 1, 2, \cdots, 4$ are bounded, but unknown. We assume that the upper bounds are $N_i > 0, i = 1, 2, \cdots, 4$ and $\dot{d}_i \leq N_i$.

Differentiating the terms in Equations (49)–(53) and combining Equations (23), (29), (35), (41) and (45) yields

$$\begin{aligned}
\dot{V}_1 &= \dot{V}_{BLF} + e_{02}\dot{e}_{02} + \varepsilon_1\dot{\varepsilon}_1 \\
&= \frac{a_0 s_1 \dot{s}_1}{k_{b1}^2 - s_1^2} + e_{02}\dot{e}_{02} + \varepsilon_1\dot{\varepsilon}_1 \\
&= \frac{a_0 s_1 \dot{x}_1}{k_{b1}^2 - s_1^2} - \frac{e_{02}^2}{\tau_2} - e_{02}\dot{x}_{2c} - \beta_1\varepsilon_1^2 + \varepsilon_1\dot{d}_1 \\
&= \frac{a_0 s_1 [b_1 x_2 + d_1]}{k_{b1}^2 - s_1^2} - \frac{e_{02}^2}{\tau_2} - e_{02}\dot{x}_{2c} - \beta_1\varepsilon_1^2 + \varepsilon_1\dot{d}_1 \\
&= \frac{a_0 s_1 [b_1(s_2 + e_{02} + x_{2c}) + d_1]}{k_{b1}^2 - s_1^2} - \frac{e_{02}^2}{\tau_2} - e_{02}\dot{x}_{2c} - \beta_1\varepsilon_1^2 + \varepsilon_1\dot{d}_1 \\
&= \frac{a_0 b_1 s_1 s_2 + a_1 b_1 s_1 e_{02} + a_1 s_1 \varepsilon_1 - a_1 k_1 s_1^2}{k_{b1}^2 - s_1^2} - \frac{e_{02}^2}{\tau_2} - e_{02}\dot{x}_{2c} - \beta_1\varepsilon_1^2 + \varepsilon_1\dot{d}_1
\end{aligned} \tag{55}$$

$$\begin{aligned}
\dot{V}_2 &= s_2\dot{s}_2 + e_{03}\dot{e}_{03} + \varepsilon_2\dot{\varepsilon}_2 \\
&= s_2[f_2(x_2) + b_2 x_3 + d_2 - \dot{x}_{2d}] + e_{03}\dot{e}_{03} + \varepsilon_2\dot{\varepsilon}_2 \\
&= s_2[f_2(x_2) + b_2(s_3 + e_{03} + x_{3c}) + d_2 - \dot{x}_{2d}] - \frac{e_{03}^2}{\tau_3} - e_{03}\dot{x}_{3c} - \beta_2\varepsilon_2^2 + \varepsilon_2\dot{d}_2 \\
&= b_2 s_2 s_3 + b_2 s_2 e_{03} + s_2\varepsilon_2 - k_2 s_2^2 - \frac{s_1 s_2}{k_{b1}^2 - s_1^2} - \frac{e_{03}^2}{\tau_3} - e_{03}\dot{x}_{3c} - \beta_2\varepsilon_2^2 + \varepsilon_2\dot{d}_2
\end{aligned} \tag{56}$$

$$\begin{aligned}
\dot{V}_3 &= s_3\dot{s}_3 + e_{04}\dot{e}_{04} + \varepsilon_3\dot{\varepsilon}_3 \\
&= s_3[f_3(x_3) + b_3 x_4 + d_3 - \dot{x}_{3d}] + e_{04}\dot{e}_{04} + \varepsilon_3\dot{\varepsilon}_3 \\
&= s_3[f_3(x_3) + b_3(s_4 + e_{04} + x_{4c}) + d_3 - \dot{x}_{3d}] - \frac{e_{04}^2}{\tau_4} - e_{04}\dot{x}_{4c} - \beta_3\varepsilon_3^2 + \varepsilon_3\dot{d}_3 \\
&= b_3 s_3 s_4 + b_3 s_3 e_{04} + s_3\varepsilon_3 - k_3 s_3^2 - \frac{e_{04}^2}{\tau_4} - e_{04}\dot{x}_{4c} - \beta_3\varepsilon_3^2 + \varepsilon_3\dot{d}_3
\end{aligned} \tag{57}$$

$$\begin{aligned}\dot{V}_4 &= s_4\dot{s}_4 + e_{05}\dot{e}_{05} + \varepsilon_4\dot{\varepsilon}_4\\ &= s_4[f_4(x_4) + b_4x_5 + d_4 - \dot{x}_{4d}] + e_{05}\dot{e}_{05} + \varepsilon_4\dot{\varepsilon}_4\\ &= s_4[f_4(x_4) + b_4(s_5 + e_{05} + x_{5c}) + d_4 - \dot{x}_{4d}] - \frac{e_{05}^2}{\tau_5} - e_{05}\dot{x}_{5c} - \beta_4\varepsilon_4^2 + \varepsilon_4\dot{d}_4\\ &= b_4s_4s_5 + b_4s_4e_{05} + s_4\varepsilon_4 - k_4s_4^2 - \frac{e_{05}^2}{\tau_5} - e_{05}\dot{x}_{5c} - \beta_4\varepsilon_4^2 + \varepsilon_4\dot{d}_4\end{aligned} \tag{58}$$

$$\begin{aligned}\dot{V}_5 &= s_5\dot{s}_5\\ &= s_5[f_5(x_5) + b_5\delta_{zc} - \dot{x}_{5d}]\\ &= -k_5s_5^2\end{aligned} \tag{59}$$

According to Equations (55)–(59), it is known that

$$\begin{aligned}\dot{V}_s =& \frac{a_0b_1s_1s_2 - s_1s_2}{k_{b1}^2 - s_1^2} + b_2s_2s_3 + b_3s_3s_4 + b_4s_4s_5 + \frac{a_0b_1s_1e_{02}}{k_{b1}^2 - s_1^2} + b_2s_2e_{03} + b_3s_3e_{04}\\ &+b_4s_4e_{05} + \frac{a_0s_1\varepsilon_1}{k_{b1}^2 - s_1^2} + s_2\varepsilon_2 + s_3\varepsilon_3 + s_4\varepsilon_4 - \frac{a_0k_1s_1^2}{k_{b1}^2 - s_1^2} - k_2s_2^2 - k_3s_3^2 - k_4s_4^2\\ &-k_5s_5^2 - \frac{e_{02}^2}{\tau_2} - e_{02}\dot{x}_{2c} - \frac{e_{03}^2}{\tau_3} - e_{03}\dot{x}_{3c} - \frac{e_{04}^2}{\tau_4} - e_{04}\dot{x}_{4c} - \frac{e_{05}^2}{\tau_5} - e_{05}\dot{x}_{5c} - \beta_1\varepsilon_1^2\\ &+\varepsilon_1\dot{d}_1 - \beta_2\varepsilon_2^2 + \varepsilon_2\dot{d}_2 - \beta_3\varepsilon_3^2 + \varepsilon_3\dot{d}_3 - \beta_4\varepsilon_4^2 + \varepsilon_4\dot{d}_4\end{aligned} \tag{60}$$

By using Young's inequality, it is known that

$$\begin{cases} s_is_{i+1} \le s_i^2 + \frac{1}{4}s_{i+1}^2\\ s_ie_{0i+1} \le s_i^2 + \frac{1}{4}e_{0i+1}^2\\ -e_{0i}\dot{x}_{ic} \le \eta_i^2e_{0i}^2 + \frac{1}{4}\\ \varepsilon_i\dot{d}_i \le N_i^2\varepsilon_i^2 + \frac{1}{4}\end{cases} \tag{61}$$

Equation (60) can be rewritten as

$$\begin{aligned}&\dot{V}_s \le \frac{(a_0b_1-1)^2}{\left(k_{b1}^2-s_1^2\right)^2}s_1^2 + \frac{1}{4}s_2^2 + b_2^2s_2^2 + \frac{1}{4}s_3^2 + b_3^2s_3^2 + \frac{1}{4}s_4^2 + b_4^2s_4^2 + \frac{1}{4}s_5^2\\ &+\frac{a_0^2b_1^2}{\left(k_{b1}^2-s_1^2\right)^2}s_1^2 + \frac{1}{4}e_{02}^2 + b_2^2s_2^2 + \frac{1}{4}e_{03}^2 + b_3^2s_3^2 + \frac{1}{4}e_{04}^2 + b_4^2s_4^2\\ &+\frac{1}{4}e_{05}^2 + \frac{a_0^2}{\left(k_{b1}^2-s_1^2\right)^2}s_1^2 + \frac{1}{4}\varepsilon_1^2 + s_2^2 + \frac{1}{4}\varepsilon_2^2 + s_3^2 + \frac{1}{4}\varepsilon_3^2 + s_4^2\\ &+\frac{1}{4}\varepsilon_4^2 - \frac{a_0k_1}{k_{b1}^2-s_1^2}s_1^2 - k_2s_2^2 - k_3s_3^2 - k_4s_4^2 - k_5s_5^2 - \frac{e_{02}^2}{\tau_2} + \eta_2^2e_{02}^2\\ &+\frac{1}{4} - \frac{e_{03}^2}{\tau_3} + \eta_3^2e_{03}^2 + \frac{1}{4} - \frac{e_{04}^2}{\tau_4} + \eta_4^2e_{04}^2 + \frac{1}{4} - \frac{e_{05}^2}{\tau_5} + \eta_5^2e_{05}^2 + \frac{1}{4} - \beta_1\varepsilon_1^2\\ &+N_1^2\varepsilon_1^2 + \frac{1}{4} - \beta_2\varepsilon_2^2 + N_2^2\varepsilon_2^2 + \frac{1}{4} - \beta_3\varepsilon_3^2 + N_3^2\varepsilon_3^2 + \frac{1}{4} - \beta_4\varepsilon_4^2\\ &+N_4^2\varepsilon_4^2 + \frac{1}{4}\\ &\le -\left[a_0k_1 - \frac{(a_0b_1-1)^2}{k_{b1}^2-s_1^2} - \frac{a_0^2b_1^2}{k_{b1}^2-s_1^2} - \frac{a_0^2}{k_{b1}^2-s_1^2}\right]\frac{s_1^2}{k_{b1}^2-s_1^2} - \left[k_2 - \frac{5}{4} - 2b_2^2\right]s_2^2\\ &-\left[k_3 - \frac{5}{4} - 2b_3^2\right]s_3^2 - \left[k_4 - \frac{5}{4} - 2b_4^2\right]s_4^2 - \left[k_5 - \frac{1}{4}\right]s_5^2 - \left[\frac{1}{\tau_2} - \frac{1}{4} - \eta_2^2\right]e_{02}^2\\ &-\left[\frac{1}{\tau_3} - \frac{1}{4} - \eta_3^2\right]e_{03}^2 - \left[\frac{1}{\tau_4} - \frac{1}{4} - \eta_4^2\right]e_{04}^2 - \left[\frac{1}{\tau_5} - \frac{1}{4} - \eta_5^2\right]e_{05}^2 - \left[\beta_1 - \frac{1}{4}\right]\varepsilon_1^2\\ &-\left[\beta_2 - \frac{1}{4}\right]\varepsilon_2^2 - \left[\beta_3 - \frac{1}{4}\right]\varepsilon_3^2 - \left[\beta_4 - \frac{1}{4}\right]\varepsilon_4^2 + 2 + N_1^2\varepsilon_1^2 + N_2^2\varepsilon_2^2 + N_3^2\varepsilon_3^2\\ &+N_4^2\varepsilon_4^2\end{aligned} \tag{62}$$

Subsequently, by selecting the design parameters as

$$\begin{aligned}\lambda = \min\Big\{ & a_0 k_1 - \tfrac{(a_0 b_1 - 1)^2}{k_{b1}^2 - s_1^2} - \tfrac{a_0^2 b_1^2}{k_{b1}^2 - s_1^2} - \tfrac{a_0^2}{k_{b1}^2 - s_1^2}, k_2 - \tfrac{5}{4} - 2b_2^2, k_3 - \tfrac{5}{4} - 2b_3^2, \\ & k_4 - \tfrac{5}{4} - 2b_4^2, k_5 - \tfrac{1}{4}, \tfrac{1}{\tau_2} - \tfrac{1}{4} - \eta_2^2, \tfrac{1}{\tau_3} - \tfrac{1}{4} - \eta_3^2, \tfrac{1}{\tau_4} - \tfrac{1}{4} - \eta_4^2, \tfrac{1}{\tau_5} - \tfrac{1}{4} - \eta_5^2, \\ & \beta_1 - \tfrac{1}{4}, \beta_2 - \tfrac{1}{4}, \beta_3 - \tfrac{1}{4}, \beta_4 - \tfrac{1}{4} \Big\}\end{aligned}$$

Equation (62) can be formulated as

$$\dot{V}_s \leq \lambda V_s + D \tag{63}$$

where $D = N_1^2 \varepsilon_1^2 + N_2^2 \varepsilon_2^2 + N_3^2 \varepsilon_3^2 + N_4^2 \varepsilon_4^2 + 2$.

Therefore, the closed-loop system is asymptotically stable, and all system states are ultimately uniformly bounded.

According to Equation (63), we can obtain

$$V_s(t) \leq V_s(0) \exp(-\lambda t) + \frac{D}{\lambda}[1 - \exp(-\lambda t)] \tag{64}$$

From Equations (19), (48) and (64), it can be further deduced that

$$\frac{1}{2} a_0 In \frac{k_{b1}^2}{k_{b1}^2 - s_1^2} \leq V_s(0) \exp(-\lambda t) + \frac{D}{\lambda}[1 - \exp(-\lambda t)] \leq V_s(0) + \frac{D}{\lambda} \tag{65}$$

Further derivation subsequently yields

$$|s_1| \leq k_{b1} \sqrt{1 - e^{-\frac{2}{a_0}[V_s(0) + \frac{D}{\lambda}]}} \tag{66}$$

Hence, there is $|s_1| < k_{b1}$. According to $|x_1| = |s_1 + x_{1d}| < k_{b1} + 0 = k_{c1}$, the BLOS angle x_1 is bounded and the FOV constraint $|x_1| < k_{c1}$ is ensured.

Hereto, the proof is completed.

Remark 3. *The proposed controller in Equation (46) for the IGC model in Equation (17) ensures that the tracking error of the closed-loop system asymptotically converges to zero and that all states of the closed-loop system are ultimately uniformly bounded. In particular, the BLOS angle constraint is ensured.*

5. Simulation Results and Analysis

To verify the effectiveness and robustness of the proposed IGC scheme for hypersonic missiles with strapdown seekers, simulations with different initial conditions, different target accelerations, and aerodynamic parameter deviations are presented in this section. The aerodynamic parameters used in this section are detailed in [28].

The initial simulation values of the missile and target are listed in Tables 1 and 2, respectively. The initial missile–target distance is $R = 5000$ m. The initial LOS angle is $q_L = 30^\circ$. The initial FOV angle is $q_B = -10^\circ$ and the maximum FOV angle is $q_B^{\max} = 20^\circ$. The minimum distance related to the dead zone of the strapdown seeker is $R_{dz} = 10$ m, and the rudder time constant and maximum rudder angle are assumed to be $\tau_z = 0.1$ and $\delta_z^{\max} = 15^\circ$, respectively.

Table 1. Initial simulation values of the missile.

(x_M, y_M)	V_M	θ_M	ϑ	α	ω_z	δ_z
$(0, 0)$	2000 m/s	35°	35°	0°	$0^\circ/s$	0°

Table 2. Initial simulation values of the target.

(x_T, y_T)	V_T	θ_T
$(2500\sqrt{3}, 2500)$	800 m/s	0°

The design parameters of the proposed controller (BLF-SMC-BC) are $k_1 = 14$, $k_2 = 15$, $k_3 = 25$, $k_4 = 25$, and $k_5 = 25$. The first-order filter parameters are $\tau_2 = 0.01$, $\tau_3 = 0.01$, $\tau_4 = 0.01$, and $\tau_5 = 0.01$. The reduced-order ESO parameters are $\beta_1 = 20$, $\beta_2 = 30$, $\beta_3 = 30$, and $\beta_4 = 1$. The desired FOV angle is assumed to be $x_{1d} = 0^\circ$.

Case 1: *If we suppose that the FOV constraint is* $k_{c1} = 20^\circ, 15^\circ, 10^\circ$ *and the maneuvering target's constant acceleration is* $a_T^Y = 50\ m/s^2$.

The simulation results are shown in Figure 3. Figure 3a–i show the missile and target trajectories, FOV angle, LOS angle, missile velocity, angle of attack, pitch angle rate, remaining intercept distance, rudder angle, and controller input, respectively. As can be observed in Table 3, the miss distance under the three constraints is less than 1 m. Figure 3b shows that the FOV angle does not exceed its maximum during the entire interception and the FOV constraint is assured under different FOV constraints. Moreover, the designed controller can ensure that the FOV angle converges rapidly to zero from its initial value and maintains it until the missile–target distance is very close, when it gradually diverges. However, the FOV angle is still within its maximum when the missile–target distance is close to the dead zone distance of the strapdown seeker. Figure 3d shows that the missile under aerodynamic drag achieves interception of a maneuvering target by its kinetic energy after losing thrust.

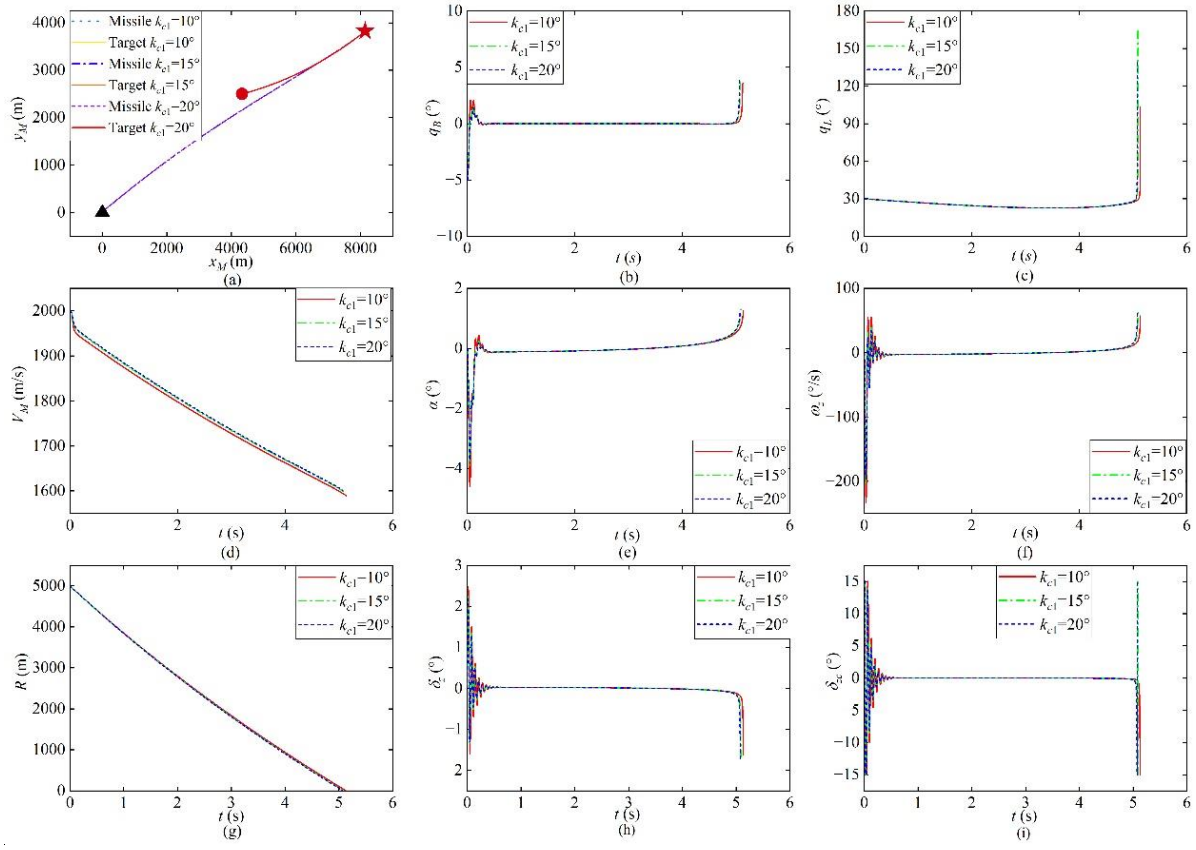

Figure 3. Simulation results under Case 1. (**a**) Missile–target pursuit trajectory. (**b**) The BLOS angle. (**c**) The LOS angle. (**d**) The velocity of missile. (**e**) The angle of attack. (**f**) The pitch angular rate. (**g**) The relative missile-target distance. (**h**) The deflection angle. (**i**) The control input.

Table 3. Simulation results under Case 1.

FOV Constraint	$k_{c1} = 10^\circ$	$k_{c1} = 15^\circ$	$k_{c1} = 20^\circ$
Miss distance	0.81 m	0.85 m	0.88 m
Interception time	5.136 s	5.092 s	5.08 s

Case 2: *If we suppose that the FOV constraint is* $k_{c1} = 20^\circ, 15^\circ, 10^\circ$ *and the sinusoidal wave acceleration of the maneuvering target is* $a_T^Y = 50\sin(0.25t)\ m/s^2$.

The simulation results are shown in Figure 4. The missile and target trajectories, FOV angle, LOS angle, missile velocity, angle of attack, pitch angle rate, remaining intercept distance, rudder angle, and controller input are shown in Figure 4a–i, respectively. From Table 4, it can be observed that the miss distance under the three constraints is less than 1 m. Similar to the simulation results in Case 2, the FOV angle can be ensured to be within the maximum FOV angle during the entire interception.

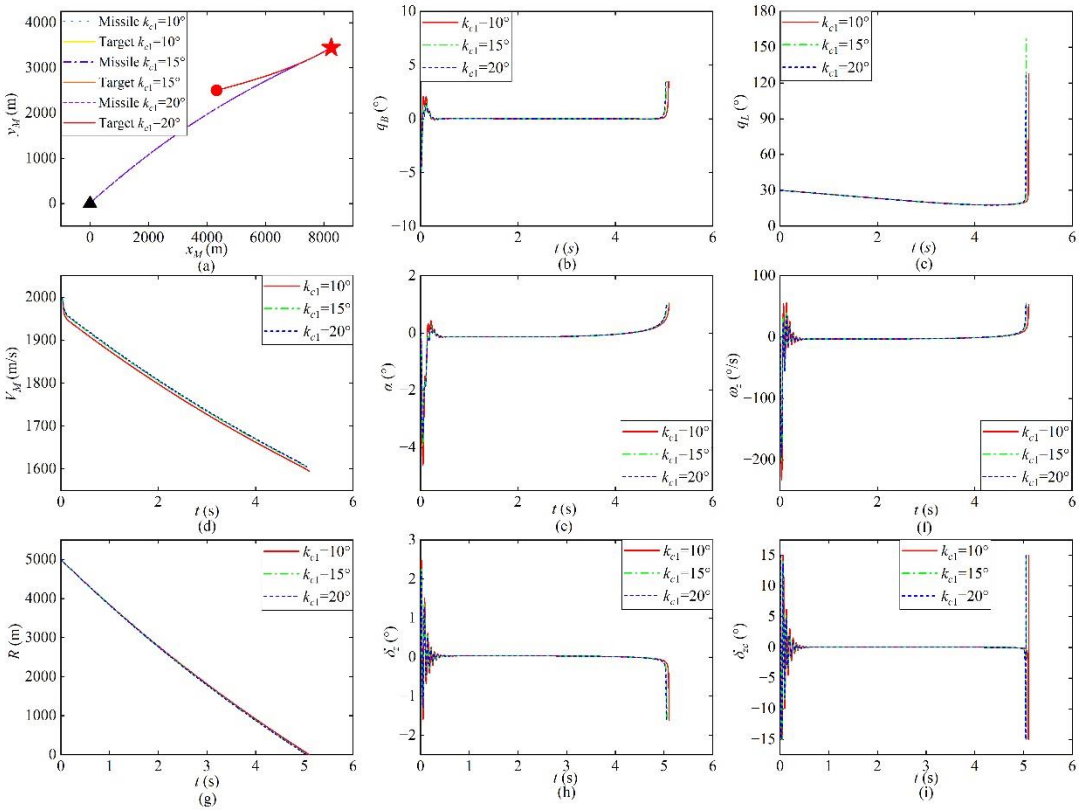

Figure 4. Simulation results under Case 2. (**a**) Missile–target pursuit trajectory. (**b**) The BLOS angle. (**c**) The LOS angle. (**d**) The velocity of missile. (**e**) The angle of attack. (**f**) The pitch angular rate. (**g**) The relative missile-target distance. (**h**) The deflection angle. (**i**) The control input.

Table 4. Simulation results under Case 2.

FOV Constraint	$k_{c1} = 10^\circ$	$k_{c1} = 15^\circ$	$k_{c1} = 20^\circ$
Miss distance	0.76 m	0.77 m	0.78 m
Interception time	5.106 s	5.062 s	5.05 s

Case 3: *Monte Carlo simulations.*

A Monte Carlo simulation is conducted to prove the robustness of the proposed IGC controller. It is planned to run 1000 samples, where the targets perform sinusoidal maneuvers. The simulation conditions for each sample in this paper are set as follows.

(1) The FOV angle constraint is generated randomly and satisfies $k_{c1} = 10^\circ \sim 20^\circ$.
(2) The normal acceleration of the target is generated randomly and satisfies $a_T = 10\sin(0.25t) \sim 50\sin(0.25\text{t})\ \text{m/s}^2$.
(3) Other biased parameters are listed in Table 5. The coefficients of the aerodynamic forces and moments are assumed to change randomly in the range of −20% to 20% of their respective nominal values.
(4) The initial values of the missile are assumed to change randomly in the range of −5% to 5%.

Table 5. Biased parameters.

Biased Parameters		Bias Value
Initial values	Pitch angle ϑ	±5%
	Flight path angle θ_M	
Aerodynamic coefficients	Drag coefficient $c_{x0}, c_x^{\alpha^2}$	±20%
	Lift coefficient $c_y^{\alpha}, c_y^{\delta_z}$	
	Pitch moment coefficient $m_z^{\alpha}, m_z^{\omega_z}, m_z^{\delta_z}$	

The 1000 Monte Carlo simulation results are shown in Figures 5–7. Figure 5 shows the BLOS angle of 1000 simulations, which indicate that the FOV angle rapidly converges to zero from its initial FOV angle and maintains it until the missile–target distance is very close, when it slowly diverges. In addition, the FOV angle does not exceed its maximum during the entire interception. The FOV angle is still within its maximum until the missile–target distance approaches the seeker's dead zone distance. Figure 6 shows the interception point distribution. A box plot of miss distance distribution is shown in Figure 7. It shows that all of the miss distances are within 0.9 m, the average is 0.48 m, and approximately 50% fall within an interval of 0.35 to 0.60 m. In summary, the Monte Carlo simulation results further demonstrate the robustness of the proposed IGC controller for intercepting high-speed maneuvering targets.

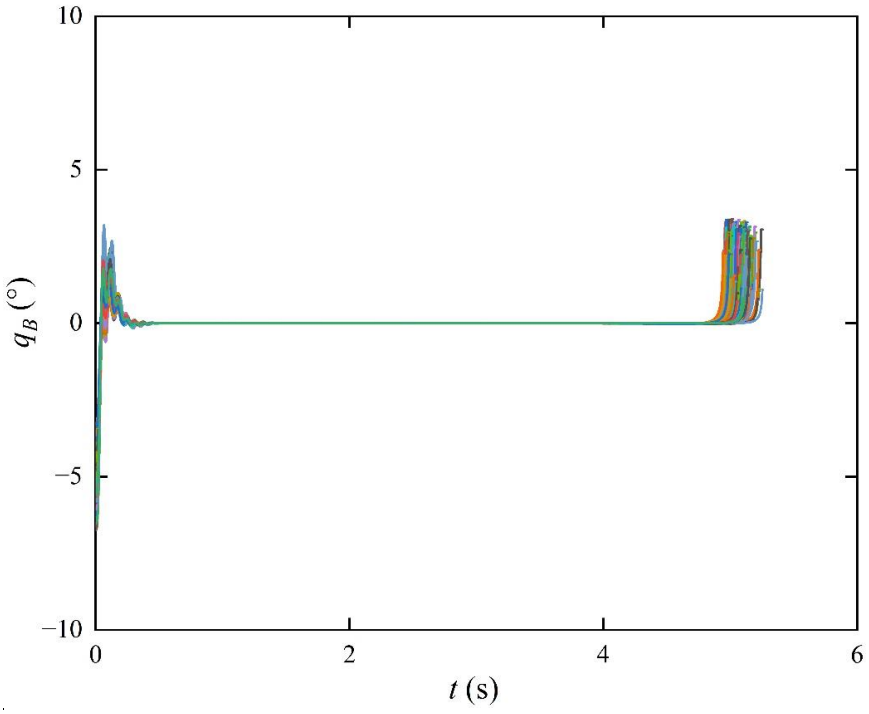

Figure 5. BLOS angles of Monte Carlo simulation under Case 3.

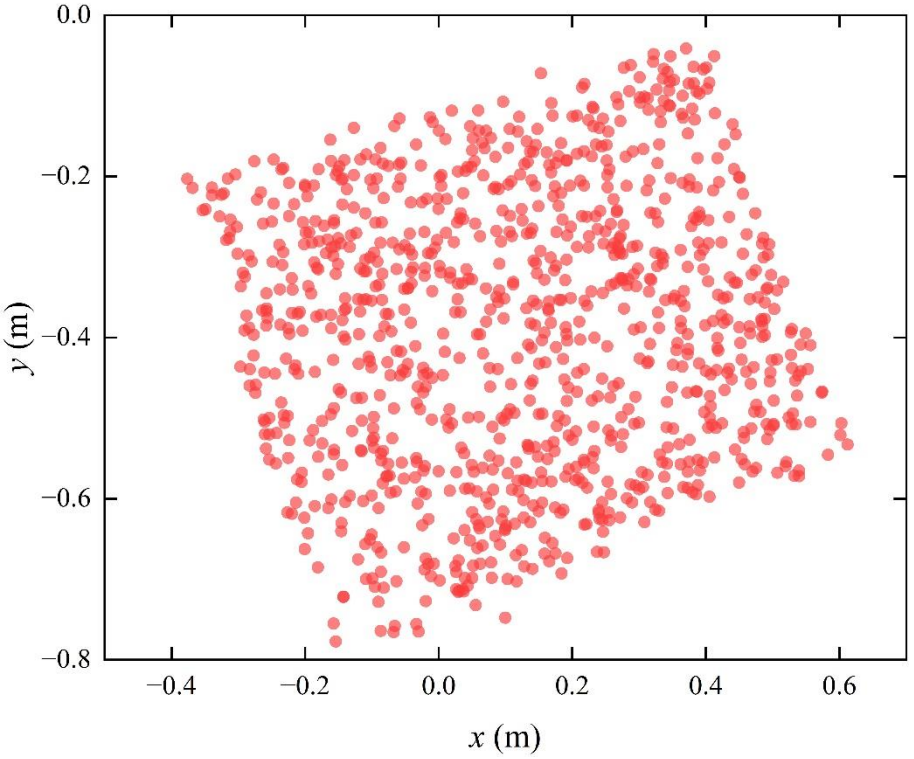

Figure 6. Interception points of Monte Carlo simulation under Case 3.

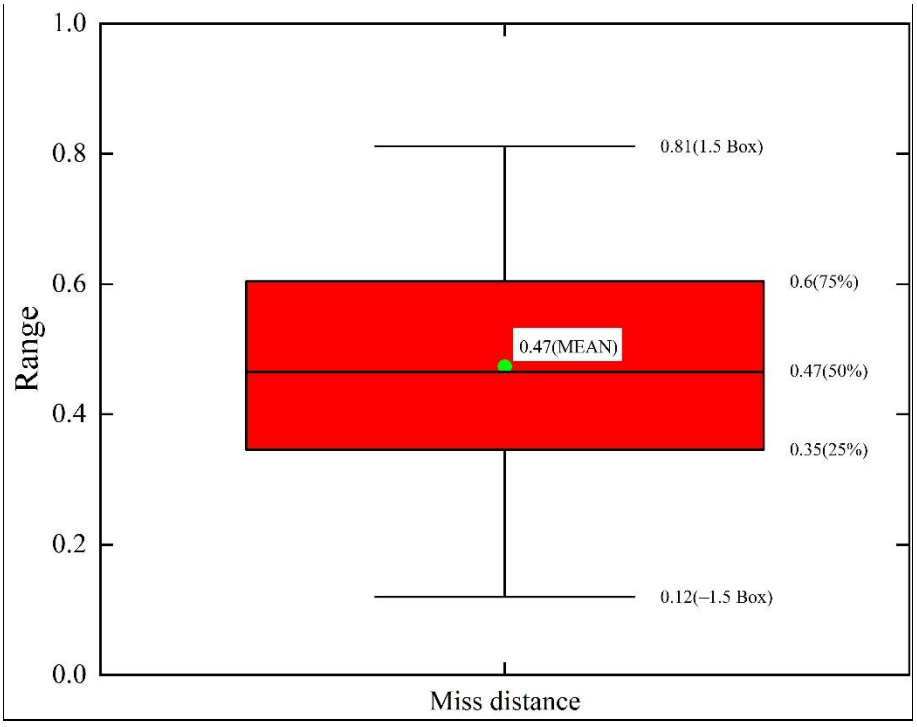

Figure 7. Miss distance of Monte Carlo simulation under Case 3.

6. Conclusions

Based on the BC, BLF, SMC, DSC, and reduced-ESO, this paper proposes a new IGC scheme with FOV constraints for a hypersonic STT missile intercepting a high-speed maneuvering target. A new fifth-order strict feedback form IGC model considering the FOV angle and rudder delay dynamics is derived considering the drag effect on axial

velocity, which most studies ignore. The BLF ensures that the FOV angle is bounded across the interception, and that the FOV constraint is realized. The DSC prevents the "differential explosion" caused by introducing virtual control commands by the BC. To improve the controller robustness, the system-lumped disturbances were estimated using the reduced-ESO and compensated in the designed controller. The simulation results under different constraints and Monte Carlo simulations demonstrate the effectiveness and robustness of the proposed IGC controller.

Adding filtering algorithms to further verify the effectiveness of the IGC controller as well as studying the IGC scheme considering the FOV constraint of the strapdown seeker in a 3D spatial coordinate system are our future research directions.

Author Contributions: Conceptualization, Z.L. and X.Z.; methodology, Z.L. and Q.D.; software, Z.L. and F.Z.; validation, Z.L., Q.D. and X.Z.; investigation, Z.L.; data curation, H.Z.; writing—original draft preparation, Z.L.; writing—review and editing, H.Z. and F.Z.; visualization, H.Z.; supervision, H.Z.; project administration, X.Z. All authors have read and agreed to the published version of the manuscript.

Funding: This research received no external funding.

Data Availability Statement: The data used in this study are available from the corresponding author upon request.

Conflicts of Interest: There are no known competing financial interests or personal relationships in this paper.

References

1. Liu, X.; Huang, W.; Du, L. An integrated guidance and control approach in three-dimensional space for hypersonic missile constrained by impact angles. *Isa Trans.* **2017**, *66*, 164–175. [CrossRef] [PubMed]
2. Yang, H.; Bai, X.; Zhang, S. Layout Design of Strapdown Array Seeker and Extraction Method of Guidance Information. *Aerospace* **2022**, *9*, 373. [CrossRef]
3. Shuang, Y.; Yanzheng, Z. A New Measurement Method for Unbalanced Moments in a Two-axis Gimbaled Seeker. *Chin. J. Aeronaut.* **2010**, *23*, 117–122. [CrossRef]
4. He, S.; Lin, D.; Wang, J. Coning motion stability of spinning missiles with strapdown seekers. *Aeronaut. J.* **2016**, *120*, 1566–1577. [CrossRef]
5. Wang, P.; Zhang, K. Research on Line-of-Sight Rate Extraction of Strapdown Seeker. In Proceedings of the 2014 33rd Chinese Control Conference (CCC), Nanjing, China, 1 January 2014; pp. 859–863.
6. Kim, H.G.; Kim, H.J. Field-of-View Constrained Guidance Law for a Maneuvering Target with Impact Angle Control. *IEEE T. Aero. Elec. Sys.* **2020**, *56*, 4974–4983. [CrossRef]
7. Kim, H.; Lee, J. Generalized Guidance Formulation for Impact Angle Interception with Physical Constraints. *Aerospace* **2021**, *8*, 307. [CrossRef]
8. Tian, J.; Bai, X.; Yang, H.; Zhang, S. Time-Varying Asymmetric Barrier Lyapunov Function-Based Impact Angle Control Guidance Law with Field-of-View Constraint. *IEEE Access* **2020**, *8*, 185346–185359. [CrossRef]
9. Liu, B.; Hou, M.; Feng, D. Nonlinear mapping based impact angle control guidance with seeker's field-of-view constraint. *Aerosp. Sci. Technol.* **2019**, *86*, 724–736. [CrossRef]
10. Zhou, S.; Hu, C.; Wu, P.; Zhang, S. Impact Angle Control Guidance Law Considering the Seeker's Field-of-View Constraint Applied to Variable Speed Missiles. *IEEE Access* **2020**, *8*, 100608–100619. [CrossRef]
11. Ma, S.; Wang, X.; Wang, Z. Field-of-View Constrained Impact Time Control Guidance via Time-Varying Sliding Mode Control. *Aerospace* **2021**, *8*, 251. [CrossRef]
12. Han, T.; Hu, Q.; Xin, M. Analytical solution of field-of-view limited guidance with constrained impact and capturability analysis. *Aerosp. Sci. Technol.* **2020**, *97*, 105586. [CrossRef]
13. Ai, X.; Wang, L.; Yu, J.; Shen, Y. Field-of-view constrained two-stage guidance law design for three-dimensional salvo attack of multiple missiles via an optimal control approach. *Aerosp. Sci. Technol.* **2019**, *85*, 334–346. [CrossRef]
14. Park, B.; Kim, T.; Tahk, M. Optimal impact angle control guidance law considering the seeker's field-of-view limits. *Proc. Inst. Mech. Eng. G J. Aerops. Eng.* **2012**, *227*, 1347–1364. [CrossRef]
15. Ming, C.; Wang, X.; Sun, R. A novel non-singular terminal sliding mode control-based integrated missile guidance and control with impact angle constraint. *Aerosp. Sci. Technol.* **2019**, *94*, 105368. [CrossRef]
16. Wang, J.; Liu, L.; Zhao, T.; Tang, G. Integrated guidance and control for hypersonic vehicles in dive phase with multiple constraints. *Aerosp. Sci. Technol.* **2016**, *53*, 103–115. [CrossRef]

17. Guo, J.; Xiong, Y.; Zhou, J. A new sliding mode control design for integrated missile guidance and control system. *Aerosp. Sci. Technol.* **2018**, *78*, 54–61. [CrossRef]
18. Jiang, S.; Tian, F.; Sun, S.; Liang, W. Integrated guidance and control of guided projectile with multiple constraints based on fuzzy adaptive and dynamic surface. *Def. Technol.* **2019**, *6*, 1130–1141. [CrossRef]
19. Li, Z.; Dong, Q.; Zhang, X.; Gao, Y. Impact angle-constrained integrated guidance and control for supersonic skid-to-turn missiles using backstepping with global fast terminal sliding mode control. *Aerosp. Sci. Technol.* **2022**, *122*, 107386. [CrossRef]
20. Zhao, B.; Xu, S.; Guo, J.; Jiang, R.; Zhou, J. Integrated strapdown missile guidance and control based on neural network disturbance observer. *Aerosp. Sci. Technol.* **2019**, *84*, 170–181. [CrossRef]
21. Tian, J.; Chen, H.; Liu, X.; Yang, H.; Zhang, S. Integrated Strapdown Missile Guidance and Control with Field-of-View Constraint and Actuator Saturation. *IEEE Access* **2020**, *8*, 123623–123638. [CrossRef]
22. Tian, J.; Xiong, N.; Zhang, S.; Yang, H.; Jiang, Z. Integrated guidance and control for missile with narrow field-of-view strapdown seeker. *Isa Trans.* **2020**, *106*, 124–137. [CrossRef] [PubMed]
23. Zhang, D.; Ma, P.; Du, Y.; Chao, T. Integral barrier Lyapunov function-based three-dimensional low-order integrated guidance and control design with seeker's field-of-view constraint. *Aerosp. Sci. Technol.* **2021**, *116*, 106886. [CrossRef]
24. Zhao, B.; Feng, Z.; Guo, J. Integral barrier Lyapunov functions-based integrated guidance and control design for strap-down missile with field-of-view constraint. *Trans. Inst. Meas. Control* **2021**, *43*, 1464–1477. [CrossRef]
25. Ames, A.D.; Coogan, S.; Egerstedt, M.; Notomista, G.; Sreenath, K.; Tabuada, P. Control Barrier Functions: Theory and Applications. In Proceedings of the 18th European Control Conference (ECC), Naples, Italy, 25–28 June 2019; IEEE: New York, NY, USA; pp. 3420–3431.
26. Shao, X.; Wang, H. Back-stepping active disturbance rejection control design for integrated missile guidance and control system via reduced-order ESO. *Isa T.* **2015**, *57*, 10–22. [CrossRef]
27. Chen, M.; Shao, S.; Jiang, B. Adaptive Neural Control of Uncertain Nonlinear Systems Using Disturbance Observer. *IEEE Trans. Cybern.* **2017**, *47*, 3110–3123. [CrossRef]
28. Chang, J.; Guo, Z.; Cieslak, J.; Chen, W. Integrated guidance and control design for the hypersonic interceptor based on adaptive incremental backstepping technique. *Aerosp. Sci. Technol.* **2019**, *89*, 318–332. [CrossRef]